

NJC

New Journal of Chemistry

Accepted Manuscript

A journal for new directions in chemistry

This article can be cited before page numbers have been issued, to do this please use: Y. Wang, B. Zhang, Z. Li, B. Wang, L. Jiao, C. Wang, L. Yang, H. Ma, L. Pang and X. Ma, *New J. Chem.*, 2020, DOI: 10.1039/D0NJ04383D.



This is an Accepted Manuscript, which has been through the Royal Society of Chemistry peer review process and has been accepted for publication.

Accepted Manuscripts are published online shortly after acceptance, before technical editing, formatting and proof reading. Using this free service, authors can make their results available to the community, in citable form, before we publish the edited article. We will replace this Accepted Manuscript with the edited and formatted Advance Article as soon as it is available.

You can find more information about Accepted Manuscripts in the [Information for Authors](#).

Please note that technical editing may introduce minor changes to the text and/or graphics, which may alter content. The journal's standard [Terms & Conditions](#) and the [Ethical guidelines](#) still apply. In no event shall the Royal Society of Chemistry be held responsible for any errors or omissions in this Accepted Manuscript or any consequences arising from the use of any information it contains.

**Efficient TiO₂/SubPc photocatalyst for degradation of organic dyes under visible
light**

Ya-Fei Wang^a, *Bing-Bing Zhang*^a, *Zhuo Li*^{a,b*}, *Bing Wang*^a, *Lin-Yu Jiao*^{a,b}, *Chen Wang*^{a,b},
Lin Yang^a, *Hai-Xia Ma*^a, *Ling-Yan Pang*^d, *Xiao-Xun Ma*^{a,b,c*}

^a School of Chemical Engineering, Northwest University, Xi'an, 710069, China

^b Chemical Engineering Research Center of the Ministry of Education for Advanced Use
Technology of Shanbei Energy, Shaanxi Research Center of Engineering Technology for
Clean Coal Conversion, Northwest University, Xi'an, 710069, China

^c International Science & Technology Cooperation Base of MOST for Clean Utilization of
Hydrocarbon Resources, Collaborative Innovation Center for Development of Energy and
Chemical Industry in Northern Shaanxi, Xi'an, 710069, China

^d School of Materials Science and Engineering, Shaanxi University of Science and
Technology, Xi'an 710021, China

1
2
3
4
5
6
7
8
9
10
11
12
13
14
15
16
17
18
19
20
21
22
23
24
25
26
27
28
29
30
31
32
33
34
35
36
37
38
39
40
41
42
43
44
45
46
47
48
49
50
51
52
53
54
55
56
57
58
59
60

Abstract:

In this work, $H_{12}SubPcB-Br$ (SubPc1) and p-hydroxybenzaldehyde were used for the synthesis of novel axially substituted subphthalocyanine $H_{12}SubPcB-OPhCHO$ (SubPc2). The photocatalyst hybrids $TiO_2/H_{12}SubPcB-OPhCHO$ ($TiO_2/SubPc2$) with different TiO_2 amounts were obtained by the solvothermal method. The structure of SubPc2 was determined by single-crystal X-ray diffraction analysis and the $TiO_2/SubPc2$ were characterized by FT-IR, UV-vis, PXRD, SEM and XPS. Furthermore, the DFT and TD-DFT calculations were studied to analyze the electronic structure and optical properties of the SubPc2. The photocatalytic degradation performance of all the samples had been evaluated by analyzing the decomposition of methyl orange (MO), bromophenol blue (BB), methylene blue (MB) and acid magenta (AM) under visible light irradiation. It was demonstrated SubPc2 acted as a role of sensitizer for pristine TiO_2 , and the optimal concentration was $TiO_2/SubPc2 = 25:1$, with the calculated rate constant value were $0.68617\ h^{-1}$, $1.41395\ h^{-1}$, $1.00701\ h^{-1}$ and $1.39237\ h^{-1}$ for MO, BB, MB and AM, respectively. The enhancement of the photocatalytic performance of $TiO_2/SubPc2$ was attributed to extend the photo-activity of the materials into the visible range and separate of photogenerated electron-hole pairs. Moreover, the photocatalytic activity of the as-prepared composite had maintained at 90.11% after five circulating degradation experiments, which was 4.5 times compared with bare TiO_2 .

Keywords: Subphthalocyanine; TiO_2 ; Photocatalysis; Degradation; DFT

1. Introduction

In recent years, the heavy reliance on various chemicals has brought serious aquatic

environmental pollution with the rapid development of the economy and industry fields.^{1,2}

The colored organic dyes are the main pollutants existing in wastewater.³ To remove organic pollutants from wastewater and improve the quality of treated wastewater discharged into the environment, the commonly used methods include chemical oxidation,⁴ adsorption technology,⁵ biological treatment and precipitation.^{6,7} However, some of these techniques are highly energy-intensive and expensive.⁸ Recently, with remarkable advantages such as environmentally friendly and high efficiency, photocatalytic technology has attracted more and more attention for its outstanding performance in water treatment.^{9,10}

TiO₂ photocatalyst has been widely used for the degradation of organic pollutants owing to its stability, non-toxicity, and high catalytic activity.^{11-Error! Reference source not found.} However, the rapid electron-hole pair recombination of TiO₂ limits its photodegradation efficiency significantly.¹⁴ Besides, pristine TiO₂ has a wide band gap (about 3.0 ~ 3.2 eV), which restricts its response to visible light.^{15,16} In order to overcome above the shortcomings and further increase the photocatalytic activity of pristine TiO₂, various strategies have been proposed, including surface modification,¹⁷ metals and non-metals dopants,¹⁸⁻²⁰ and dye sensitization.²¹ The phthalocyanines (Pcs) species have been introduced to sensitize TiO₂ owing to its stable and high hole mobility as well as low cost.^{22,23} More recently, the studies reported by Li et al. have shown that tetra-nitro-phthalocyanine Copper (II) sensitized TiO₂ have remarkable light absorption ability.²⁴

Subphthalocyanines (SubPcs) are non-planar aromatic macrocyclic molecular structure related to Pcs, consisting of three isoindole units connected by three nitrogen bridges, with a central boron atom linked with axial substituents.^{25,26} This unique makeup gives rise to a 14

1
2
3
4 π -electron aromatic system with specific characteristics, like the high carrier mobility and
5
6
7 high quantum yields of fluorescence.^{Error! Reference source not found.-29} The recent studies on the
8
9
10 SubPcs were mainly devoted to their unique optical and electrochemical properties, and they
11
12 have shown great potential for application in organic light-emitting diodes (OLEDs), organic
13
14 solar cells (OSCs) and nonlinear optics.³⁰⁻³¹ However, there are few reports of
15
16 SubPc-sensitized semiconductor materials and used for photodegradation of organic
17
18
19
20 pollutants present in water.

21
22
23 In this paper, a novel p-hydroxybenzaldehyde phenoxy substituted subphthalocyanine
24
25 (SubPc2) was fabricated using a simple solvothermal method. Based on the sensitizer
26
27 synthesis, TiO₂/SubPc2 photocatalysts with different SubPc2 mass ratios were prepared by a
28
29 solvothermal method. The photocatalytic activity of catalysts was investigated by the
30
31 degradation of methyl orange (MO), bromophenol blue (BB), methylene blue (MB) and acid
32
33 magenta (AM) under visible light irradiation. We have computed the electronic structure and
34
35 optical properties of the SubPc2 using DFT and TD-DFT. Based on the calculations and
36
37 experiment results, a possible photocatalytic mechanism of the TiO₂/ SubPc2 composite was
38
39
40
41 given. This novel water purification strategy provides a new idea for the design and
42
43 development of high-efficiency photocatalyst in the future.

44 45 46 47 48 **2. Experimental and computational methods**

49 50 51 **2.1. Materials and instrumentation**

52
53
54 All chemicals were obtained from commercial suppliers and were used as received
55
56 without further purification unless otherwise indicated.

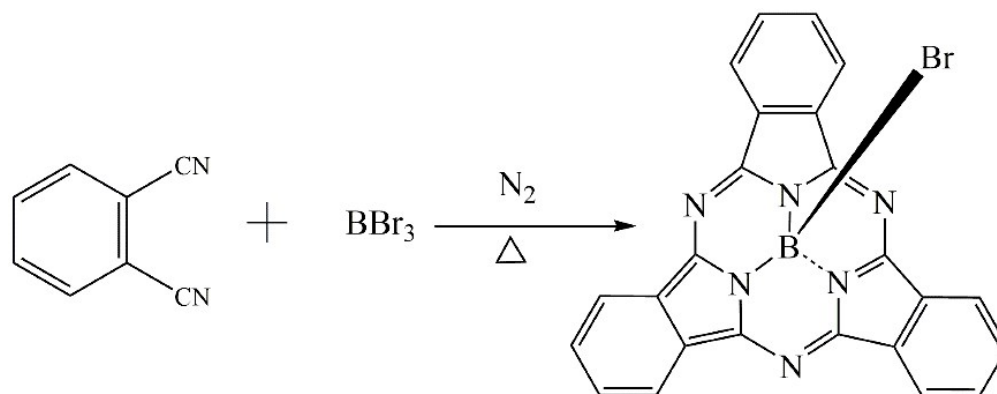
57
58
59 UV-vis spectra data were recorded on a Specord 200 instrument using toluene as a
60

reference. Fourier transform infrared (FT-IR) spectroscopy ($400 \sim 4000 \text{ cm}^{-1}$) of materials was carried out at room temperature using a Bruker Vect 002. The morphology of the composites was studied by scanning electron microscopy (SEM) in a SIGMA instrument. Powder X-ray diffraction (PXRD) analysis was performed in a Bruker D/Max-III using $\text{Cu K}\alpha$ radiation ($\lambda=1.5414 \text{ \AA}$). X-ray photoelectron spectroscopy (XPS) was carried out using a Kratos AXIS NOVA spectrometer.

2.2. Synthesis

2.2.1. SubPc1

As shown in scheme 1, the parent subphthalocyanine $\text{H}_{12}\text{SubPcB-Br}$ (SubPc1) was synthesized based on previously reported literature.³² The target subphthalocyanine SubPc1 was obtained as a dark purple solid. Yield: 1.596 g (62.3%).



Scheme 1. Synthetic route of SubPc1

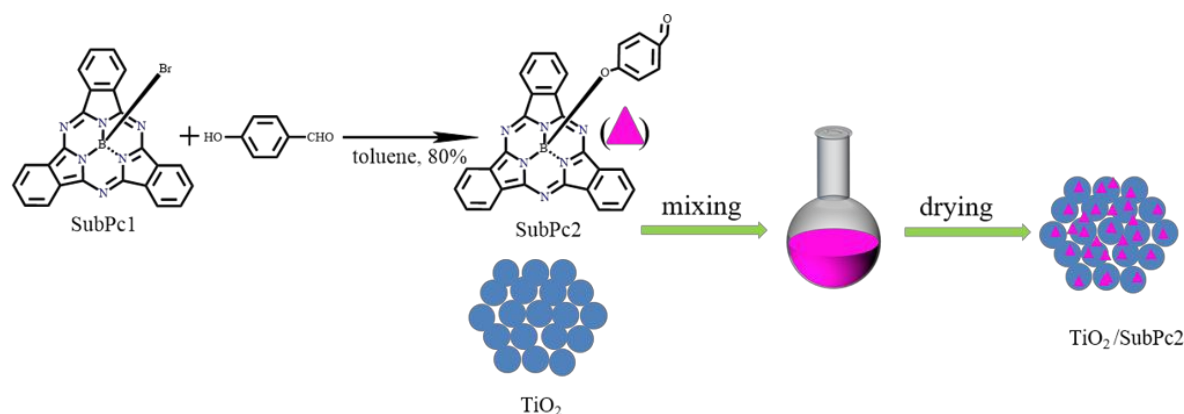
2.2.2. SubPc2

The new axially substituted subphthalocyanine SubPc2 was synthesized according to the Scheme 2. The parent subphthalocyanine SubPc1 (0.05 mmol, 0.02375 g) and *p*-hydroxybenzaldehyde (0.1 mmol, 0.012 g) were dissolved in 6 mL of toluene. The reaction mixture was stirred for 30 min under room temperature, and then 2 drops of pyridine were

added to adjust the pH value. The completely dissolved mixture was transferred into a 25 ml Teflon-lined stainless autoclave and placed in the oven. The oven thermal gradient rose from an initial 25 °C to 130 °C at 10.5 °C/h, kept in a 130 °C oven for 72 h, and cooled down to room temperature at a rate of 5 °C/h to ensure complete crystallization. The solvent was evaporated by using a rotary evaporator to get the purplish-red crude extract, which was washed with n-alkane, dichloromethane, chloroform and ethanol, respectively. The insoluble portion was filtered by a glass funnel and dried in a vacuum for 24 h. Yield: 0.0154 g (43.2%).

2.2.3. TiO₂/SubPc2 composites

To prepare TiO₂/SubPc2, SubPc2 (25 mg) was first dissolved in 50 mL toluene and stirred for 3 h at room temperature. A certain amount of TiO₂ (0.625g, 1.25g, 1.875g, 2.5g, 5g) was added into the above solution and thoroughly mixed followed by bath sonication for 3 h in the dark. The solvent was removed by a rotary evaporator at 60 °C form a light-purple powder which was subsequently dried under vacuum to obtain TiO₂/SubPc2 composites. Following the above procedure, the TiO₂/SubPc2 composites were prepared and their different mass ratios were 25:1, 50:1, 75:1, 100:1 and 200:1. All operations are performed in the dark.



Scheme 2. Schematic diagram of the synthesis of SubPc2 and TiO₂/SubPc2

2.3. X-ray Crystal Structure Determination

X-ray single diffraction was measured through Bruker SMART APEX CCD X-ray diffractometer equipped with graphite-monochromatized Mo-K α radiation ($\lambda = 0.071073$ nm) by using a ϕ - ω scan mode at 296 (2) K. The single-crystal structures were solved by the direct method using SHELXTL-97 and all the non-hydrogen atoms were refined by full-matrix least-squares techniques on F² with anisotropic thermal parameters. Crystallographic data of the SubPc2 were summarized in Supporting Information Table 1.

2.4. Computational methods

To have a better understanding electronic structure of SubPc2, we have performed a series of DFT and TD-DFT calculations using B3LYP/6-31G methods with the Gaussian 16³³ software package. Frequency calculations were performed on all optimized shapes to ensure that the resulted structures represent the local minimum. VMD software³⁴ was used for molecular visualization and the molecular orbitals were drawn with the isodensity surfaces (0.02 a.u). Electrostatic potential surfaces (ESP) were performed using Gaussian View. Atomic orbitals contributions were calculated with the Multiwfn³⁵ program package.

2.5. Photodegradation reaction

The measurement of photocatalytic activity was evaluated by the degradation of MO, BB, MB and AM under visible light irradiation. The light source used was a CEL-HXF300 xenon lamp with a filter to remove the irradiation of $\lambda < 400$ nm. In the photocatalytic degradation process, 0.1 g of the photocatalyst was solved in 50 mL of organic dye solution (10 mg/L) by an ultrasound water bath at room temperature for 1 h. Before illumination, the

1
2
3
4 resulting solution was stirred in the dark for 30 min to ensure the establishment of
5
6
7 adsorption-desorption. During illumination, the distance between the light source and the
8
9
10 solution was kept constant at 10 cm. About 5 mL of the aqueous solution was collected and
11
12 filtered out from the reactor vessel at every 30 min interval of time for UV-vis spectroscopic
13
14 analysis. For the cycling experiment, the photocatalyst was separated from the degraded
15
16 solution, they were washed by distilled water and ethanol, and then dried at 60 °C for 1 h.
17
18
19
20

21 22 **3. Results and discussion**

23 24 **3.1. Crystal structure and characterization**

25
26 The crystal structures of SubPc2 obtained by X-ray analysis were shown in Fig. 1. To
27
28 clarity, the crystal data were summarized in Table S1 (Supporting Information), and the
29
30 geometry parameters including bond and bond length are listed in Table S2. As previously
31
32 reported for a wide range of SubPcs,³⁶ the boron atom is coordinated with three nitrogen and
33
34 one oxygen atoms in a tetrahedral geometry, resulting in a stable bowl-shaped conical
35
36 conformation. Data were shown that SubPc2 belongs to the single-crystal system and *P21/n*
37
38 space group, and $a, b, c, \alpha, \beta, \gamma = 15.606(3) \text{ \AA}, 9.991(2) \text{ \AA}, 16.737(4) \text{ \AA}, 90^\circ, 111.846^\circ, 90^\circ,$
39
40
41 respectively. The distance between the boron atom of the macrocycle and oxygen atoms of
42
43 axial position (B1-O1) is 1.46 Å. The dihedral angles of the SubPc2 containing N1, N3 and
44
45 N5 atoms with the (N_p)₃ plane are 110.8°, 115.6° and 115.5°, respectively.
46
47
48
49
50
51
52
53
54
55
56
57
58
59
60

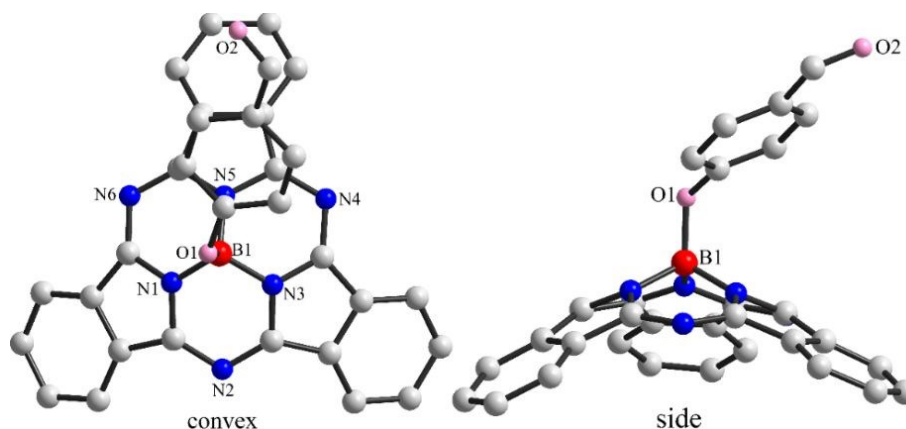


Fig. 1. Structure of SubPc2 (C, gray; N, blue; B, red; O, pink).

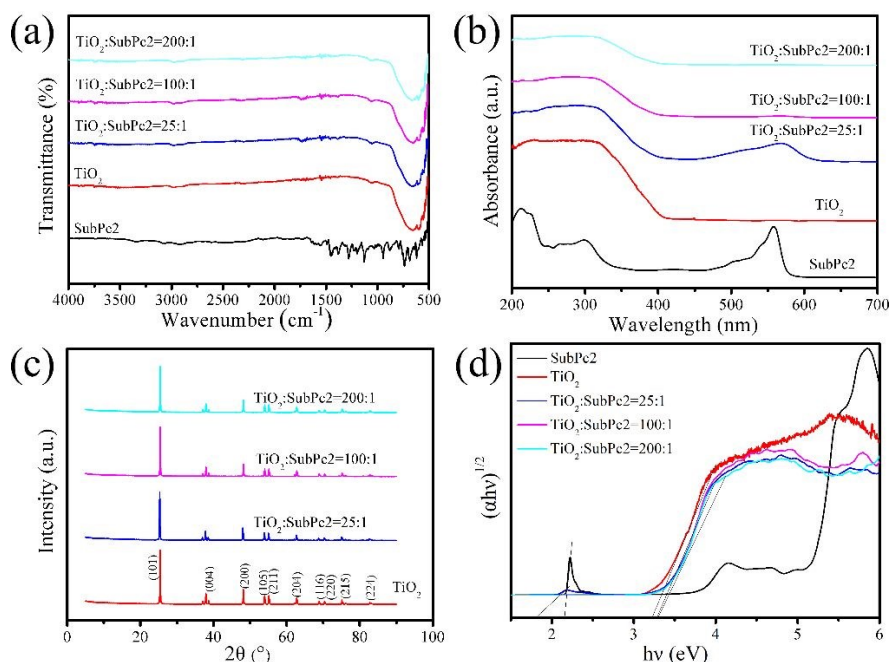


Fig. 2. (a) FT-IR spectra of the SubPc2, TiO₂ and TiO₂/SubPc2. (b) UV-vis spectrum of the SubPc2, TiO₂ and TiO₂/SubPc2. (c) PXRD diffraction patterns of the TiO₂ and TiO₂/SubPc2. (d) Corresponding transformed the Kubelka-Munk plot of SubPc2, TiO₂ and TiO₂/SubPc2.

The FT-IR spectrum analysis of SubPc2 was shown in Fig. 2 (a). The band at 1610 cm⁻¹ can be attributed to the stretching vibration of C=C. The vibration peaks at 954 cm⁻¹, 963 cm⁻¹, and 724 cm⁻¹ belonging to the macrocycle framework of SubPc2. The appearance of

stretching vibrations of C=N in SubPc2 at 1499 cm^{-1} . The peak around 600 cm^{-1} is attributed to the Ti-O vibrational mode. Besides, the vibration of Ti-O functional groups in all catalysts was monitored near 600 cm^{-1} , indicating that doping between TiO_2 and SubPc2 occurred.

As shown in Fig. 2 (b), the UV-vis spectrum of the SubPc2 exhibited the expected two main transitions, the B- band between 250 ~ 350 nm and the long wave Q- band between 450 ~ 620 nm, which is typical for SubPc and their macrocycle analog.³⁷ The TiO_2 showed an obvious absorption of light below 400 nm, which means the strong UV light absorption in the ultraviolet region of the TiO_2 . Compared with pure TiO_2 , the TiO_2 /SubPc2 composites absorb both in the UV and the visible region. The effective light absorption in the visible and ultraviolet region would be favorable for enhancing the photodegradation ability of TiO_2 /SubPc2 with different concentrations.

PXRD revealed that the main structural features of TiO_2 and TiO_2 /SubPc2. As illustrated in Fig. 2 (c), the characteristic diffraction peaks at 25.23°, 37.8° and 48.1° could be ascribed to the (101), (004) and (200) facets of the planes of anatase TiO_2 (JCPDS NO. 84-128), respectively. For the TiO_2 /SubPc2 composites at the different concentrations, the recorded diffraction patterns did not observe extra featured summits that can be explained for the lower concentrations of SubPc2. In other words, the addition of the SubPc2 has no change in the crystal structure of TiO_2 , indicating that SubPc2 was successfully loaded onto surface TiO_2 .

The bandgap energies of these samples can be calculated by plotting the transformed Kubelka–Munk function, as shown in Fig. 2 (d). The band gaps of pure TiO_2 and SubPc2 are 3.25 eV and 2.17 eV, respectively. With the increase of SubPc2, the bandgap of the sample (TiO_2 :SubPc2 = 25:1) reached a minimum value of 1.8 eV. The narrow bandgap of catalysts

may make it enhance photoresponse in the UV and visible range of the spectrum. Moreover, the narrow bandgap is beneficial for the photogenerated electrons transfer from the VB to the CB, which can increase the carrier concentration. These are favorable to the photodegradation of pollutants.

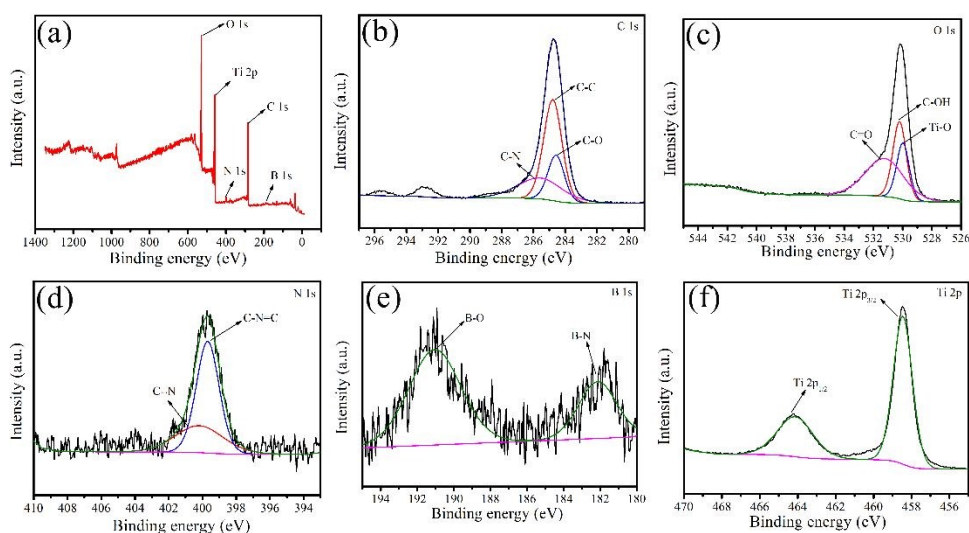


Fig. 3. XPS spectra of $\text{TiO}_2/\text{SubPc}2$: (a) the survey spectrum, (b) C 1s peak, (c) O 1s peak, (d) N 1s peak, (e) B 1s peak, (f) Ti 2p peak.

X-ray photoelectron spectroscopy (XPS) spectra were performed to analyze the surface elemental composition of the $\text{TiO}_2/\text{SubPc}2$ photocatalysts. According to the XPS survey scan shown in Fig. 3 (a), the XPS peaks for the elements C, O, N, B and Ti can be clearly observed for the $\text{TiO}_2/\text{SubPc}2$ samples. In Fig. 3 (b), the C 1s XPS spectra located at binding energies of 284.7 (C1), 286.3 (C2) and 285.8 eV (C3) were ascribed to CC-, CN- and CO- bonds, respectively. As shown in Fig. 3 (c), there are three different O 1s characteristic peaks located at 529.9 eV, 530.8 eV and 521.7 eV, corresponding to three different kinds of O chemical states, which are the lattice oxygen (Ti-O), external hydroxyl groups (C-OH) and C=O bands, respectively. As shown in Fig. 3 (d), two peaks of N 1s located at 399.2 eV and 400

1
2
3
4 eV were observed and can be attributed to the C-N=C and N atom coordination bonding with
5
6
7 B atom, respectively. For the B 2s spectra shown in Fig. 3 (e), the peaks at 191 eV and 182
8
9
10 eV can be assigned to B-O and B-N, respectively. In Fig. 3 (f), XPS peaks at a binding energy
11
12 of 458.4 eV and 464.1 eV can be ascribed to Ti 2p_{3/2} and Ti 2p_{1/2}, respectively. The above
13
14 XPS result analysis also indicates the successful synthesis of SubPc2 on the TiO₂ by the
15
16 solvothermal method.
17
18
19
20
21
22
23
24
25
26
27
28
29
30
31
32
33
34
35
36
37
38
39
40
41

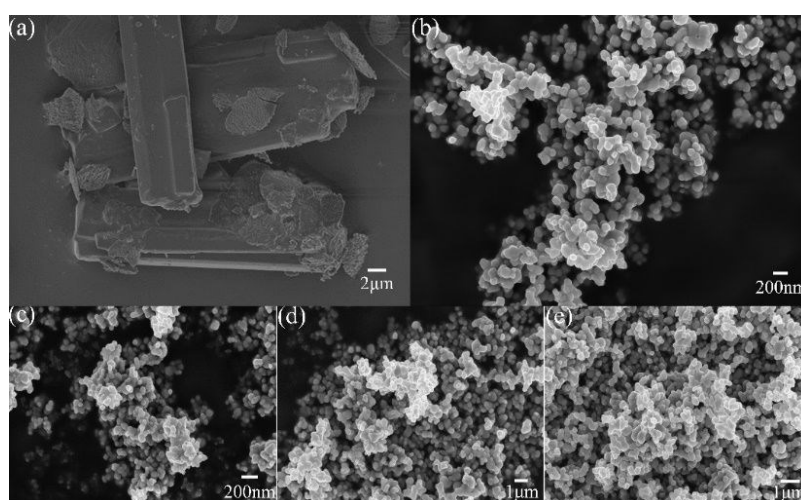


Fig. 4. SEM images of samples obtained from (a) SubPc2, (b) TiO₂, (c)TiO₂/SubPc2 (25:1),
(d)TiO₂/SubPc2 (100:1), (e)TiO₂/SubPc2 (200:1).

42 SEM measurements were used for the investigation of surface microscopic morphology
43
44 of all catalysts. Fig. 4 showed representative SEM images of SubPc2, TiO₂ and their
45
46 composites TiO₂/SubPc2. Form Fig. 4 (a), the SubPc2 is composed of many particles which
47
48 with flake shape and smooth surface. As shown in Fig. 4 (b), the pure TiO₂ aggregated to
49
50 larger particles by the small and spherical-like particles. Compared with pure TiO₂, all the
51
52 composite materials showed big particle-like morphology which was closely packed together.
53
54
55 With the increase of SubPc2, the agglomeration phenomenon is gradually reduced, which was
56
57
58
59
60

beneficial to increase the surface area of TiO₂ and enhance the photocatalytic efficiency.

Furthermore, to investigate the correlations between TiO₂ and SubPc2, the sample of TiO₂/SubPc2 was tested by Raman technique. Raman spectra in the range of 100-900 cm⁻¹ for TiO₂ and TiO₂/SubPc2 photocatalysts are shown in Fig. S1. The Raman peaks were observed at 144.7, 398.2, 517.1 and 639.8 cm⁻¹ in the pure TiO₂, indicating the anatase phase of TiO₂ which is consistent with XRD analysis. Moreover, a new weak peak appeared around 703.5 cm⁻¹ indicates that the successful combination of TiO₂ and SubPc2.

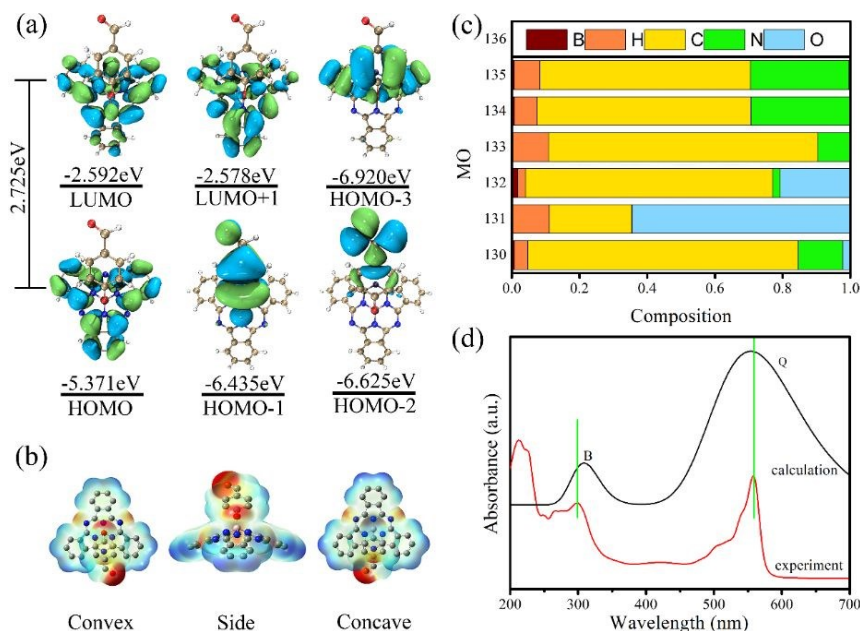


Fig. 5. (a) Partial molecular orbital diagram of SubPc2. (b) Electrostatic potential surfaces of SubPc2. (c) Analysis of the orbital compositions. (d) Experimental and calculated UV-vis spectra of SubPc2.

The partial molecular orbital diagrams of SubPc2 were shown in Fig. 5 (a) and part of the transition state information was summarized in Table 1. From the figure we can see that HOMO-1, HOMO-2 and HOMO-3 are mainly located on the parent SubPc and axial organic molecular ligand. Meanwhile, HOMO, LUMO, LUMO+1 are located on the parent

subphthalocyanine skeleton, which causes fast electron-hole separation. The absorption peak at 502.89 nm was mostly contributed to transit from HOMO to LUMO and the HOMO-LUMO energy gap of SubPc2 is 2.725 eV. Electrostatic potential surfaces (ESP) analysis of SubPc2 showed in Fig. 5 (b), where the red, blue and green areas regions represent the positive, negative and neutral values, respectively. It can be seen from the figure that the red region is mainly axial electron-rich oxygen atoms, showing the highest negative ESP value in the convex view. The blue area is mainly a large axial ring on the periphery, showing a positive ESP value in the concave view containing boron atoms. The higher difference between negative and positive charge accumulation indicates that SubPc2 may act as acceptor and donor when reacting within and between molecules. Experimental and calculated UV-vis spectra of SubPc2 were shown in Fig. 5 (d). Compared with the experimental spectrum, the calculated B- band is blue-shifted and Q- band is slightly red-shifted. The calculation can reproduce features of the experimental observed in UV-vis spectra for SubPc2.

Table 1. Excitation Energies and transition orbital contribution based on CAM-B3LYP functional with 6-31G* as basis sets. ($f > 0.1$)

State	Excitation energy (eV)	λ (nm)	Transition Orbital (contribution)	Oscillator strengths (f)
1	2.4561	504.80	129->135 (21.79%)	$f=0.4392$
			133->134 (95.82%)	
2	2.4654	502.89	129->134 (21.80%)	$f=0.4640$
			133->135 (95.68%)	
9	4.4546	278.33	124->135 (6.409%)	$f=0.1257$
			132->135 (72.24%)	
			133->137 (12.47%)	

3.2. Photocatalytic degradation

SubPc2 was mixed with TiO₂ with five different concentrations to select the optimum concentration for photocatalytic degradation. The photocatalytic activity of the TiO₂/SubPc2 composites was studied by the degradation of MO, BB, MB and AM under visible light irradiation. The characteristic absorption peaks of MO, BB, MB and AM are at 463, 592, 665 and 542 nm, respectively. The degradation effect of the pollutants can be calculated by the following equation: $\text{Rate} = \frac{A_0 - A}{A_0} \times 100\% = \frac{C_0 - C}{C_0} \times 100\%$,³⁸ where A₀ and A represent the primary and time-dependent absorbance of the sample, C₀ and C represent the primary and time-dependent concentration of the sample. Furthermore, the photodegradation of the organic pollutants can be regarded as a pseudo first-order kinetics reaction and the rate constant is calculated by the following equation: $\ln\left(\frac{C}{C_0}\right) = -kt$,³⁹ where k is rate constant.

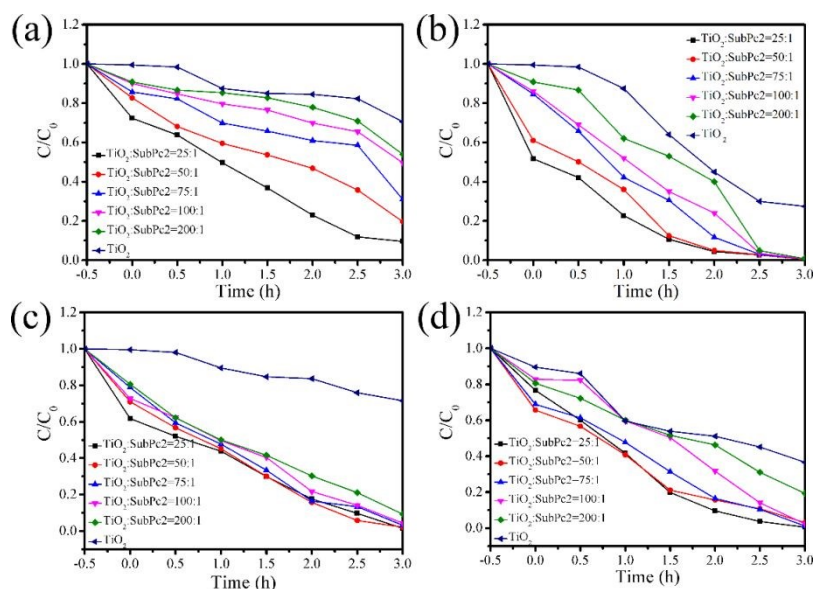


Fig. 6. Photocatalytic degradation of a) MO, b) BB, c) MB and d) AM under visible light irradiation.

The degradation efficiency of the pure TiO₂ and TiO₂/SubPc2 for four organic dyes

under visible light irradiation within 3 h was shown in Fig. 6. As shown in Fig. 6, the photocatalytic performance of pure TiO₂ were merely 29.4%, 72.5%, 27.6% and 64.38% for MO, BB, MB and AM degradation under visible light irradiation within 3 h, respectively. For MO degradation, the photodegradation activity of the samples follows the sequence (Fig. 6 a): TiO₂:SubPc2=25:1 (90.4%) > TiO₂:SubPc2=50:1 (80.4%) > TiO₂:SubPc2=75:1 (69.7%) > TiO₂:SubPc2=100:1 (50.4%) > TiO₂:SubPc2=200:1 (46.1%) > pure TiO₂ (29.4%). Similar results were acquired for other three pollutants degradation under visible light irradiation. For BB degradation, the photodegradation activity of the samples follows the sequence (Fig. 6 b): TiO₂:SubPc2=25:1 (99.5%) = TiO₂:SubPc2=50:1 (99.5%) > TiO₂:SubPc2=75:1 (99.3%) = TiO₂:SubPc2=100:1 (99.3%) > TiO₂:SubPc2=200:1 (99.2%) > pure TiO₂ (72.5%). For MB degradation, the photodegradation activity of the samples follows the sequence (Fig. 6 c): TiO₂:SubPc2=25:1 (98.5%) > TiO₂:SubPc2=50:1 (97.9%) > TiO₂:SubPc2=75:1 (96.8%) > TiO₂:SubPc2=100:1 (95.7%) > TiO₂:SubPc2=200:1 (90.7%) > pure TiO₂ (27.6%). For AM degradation, the photodegradation activity of the samples follows the sequence (Fig. 6 d): TiO₂:SubPc2=25:1 (99.5%) > TiO₂:SubPc2=75:1 (98.8%) > TiO₂:SubPc2=100:1 (97.7%) > TiO₂:SubPc2=50:1 (96.9%) > TiO₂:SubPc2=200:1 (80.7%) > pure TiO₂ (64.83%). These results showed that all the photodegradation rates had increased with the addition of different mass ratios of SubPc2. In compared with pure TiO₂, the degradation rate of TiO₂/SubPc2 (25:1) towards MO, MB is enhanced about 3 times, and about 1.5 times for BB and AM. For all organic dyes, the optimal photodegradation ratio is TiO₂:SubPc2=25:1. It may be the aggregation and agglomeration of the TiO₂ was reduced on the surface of the composite (seen by SEM image), which may have increased the effective surface area and visible light

irradiation for the samples. The BET surface area was investigated by a N_2 adsorption-desorption analysis, as shown in Fig. S2. A higher BET surface area ($9.8186 \text{ m}^2/\text{g}$) of $TiO_2/\text{SubPc}2$, compared with the TiO_2 ($9.5724 \text{ m}^2/\text{g}$) was observed, which might be the result of the increased of the pore structure after the mixing. It was found that BB percentage degradation is faster than other organic dyes, which may be attributed to the self-degradation under the visible light irradiation.

To better study the photocatalytic performance, the date of the pseudo first-order kinetic rate constant (k) is summarized in Table 2. The degradation rate constants of TiO_2 for MO, BB, MB and AM are 0.09211 h^{-1} , 0.42121 h^{-1} , 0.1007 h^{-1} and 0.28842 h^{-1} , respectively. The values of release rate constants increased with the addition of SubPc2. It can be seen that SubPc can sensitize TiO_2 and improve its photocatalytic performance.

Table 2. Pseudo first-order kinetic rate constant (k) of the organic pollutants degradations.

k (h^{-1})	MO	BB	MB	AM
TiO_2	0.09211	0.42121	0.1007	0.28842
$TiO_2:\text{SubPc}2=25:1$	0.68617	1.41395	1.00701	1.39237
$TiO_2:\text{SubPc}2=50:1$	0.40079	1.43967	1.04347	0.90115
$TiO_2:\text{SubPc}2=75:1$	0.26329	1.3556	0.88471	1.06606
$TiO_2:\text{SubPc}2=100:1$	0.16952	1.29297	0.80006	0.91159
$TiO_2:\text{SubPc}2=200:1$	0.14077	1.21124	0.61115	0.42287

Additionally, we also examined the total organic carbon (TOC) content of the BB and MB degradation solutions during the 3h irradiation time. The experimental result was shown

 1
2
3
4
5
6
7
8
9
10
11
12
13
14
15
16
17
18
19
20
21
22
23
24
25
26
27
28
29
30
31
32
33
34
35
36
37
38
39
40
41
42
43
44
45
46
47
48
49
50
51
52
53
54
55
56
57
58
59
60

in Fig. S3. The results indicated that the TOC removal efficiency of BB and MB finally reaches 56.1% and 52.2%, respectively. The photocatalyst sensitized by SubPc2 has high salinity mineralization.

Table 3. Comparison with other photocatalysts to degrade bromophenol blue.

Photocatalysts	Pollutant concentration (mg·L ⁻¹)	Dosage (g·L ⁻¹)	Degradation time (min)	Degradation rate	Ref
silver nanoparticles supported on cellulose	10	0.1	60	90.9%	40
AgBr-ZnO	7	0.15	50	89.3%	41
MNPs	20	0.2	60	98%	42
GNP-PPy (50%)	20	0.5	120	93%	43
Nb ₂ O ₅	6	0.4	120	80	44
Co ₃ O ₄ NPs	100	0.2	40	95%	45
TiO ₂	10	0.1	180	72.5%	this work
TiO ₂ :SubPc2=25:1	10	0.1	180	99.5%	this work

The photocatalytic degradation of bromophenol blue aqueous solution with different photocatalysts is described in Table 3. It can be seen from the table that, all the photocatalysts were able to degrade bromophenol blue over 70%. In our study, the degradation rates of the TiO₂/SubPc2 catalysts can reach 99.5%. The comparison shows that the catalyst of our prepared has great potential in degrading BB.

To further clarify the proposed reaction mechanism of the TiO₂/SubPc2 photocatalyst, a series of radical scavenging experiments were carried out in the reaction system to confirm the active species in the photocatalytic process. The ethylenediaminetetraacetic acid disodium

 1
2
3
4
5
6
7
8
9
10
11
12
13
14
15
16
17
18
19
20
21
22
23
24
25
26
27
28
29
30
31
32
33
34
35
36
37
38
39
40
41
42
43
44
45
46
47
48
49
50
51
52
53
54
55
56
57
58
59
60

salt (EDTA, 10 mmol·L⁻¹), isopropanol (IPA, 10 mmol·L⁻¹) and benzoquinone (BQ, 10 mmol·L⁻¹) were used to trap h⁺, ·OH and ·O₂⁻, respectively. It was obviously shown that photocatalytic efficiency of BB decrease when EDTA, IPA and BQ were present in the solution, implying the important role of h⁺, ·OH and ·O₂⁻ in the degradation (Fig. S4).

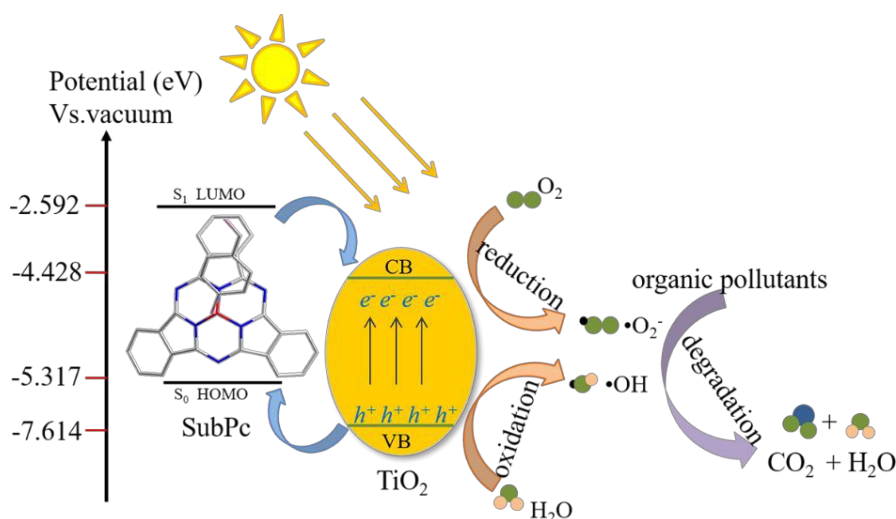


Fig. 7. Possible degradation mechanism of TiO₂/SubPc₂ composites.

The mechanism of degrading organic pollutants can be described in Fig. 7. After excitation by the incident light, both photocatalysts can generate electron-hole pairs. The photogenerated electrons were transferred from LUMO of SubPc to CB of TiO₂, while photogenerated holes transferred in the opposite direction. Consequently, electrons and holes accumulated on CB of TiO₂ for reduction reactions and SubPc for oxidation reactions, respectively. The electrons of CB-TiO₂ could reduce O₂ into ·O₂⁻ and the holes of HOMO-SubPc could oxidize OH⁻ into ·OH. These produced active species (·O₂⁻, ·OH, and h⁺) could degrade the organic pollutants into CO₂, H₂O, achieving highly efficient organic pollutants photodegradation.

3.3. Reusability and stability

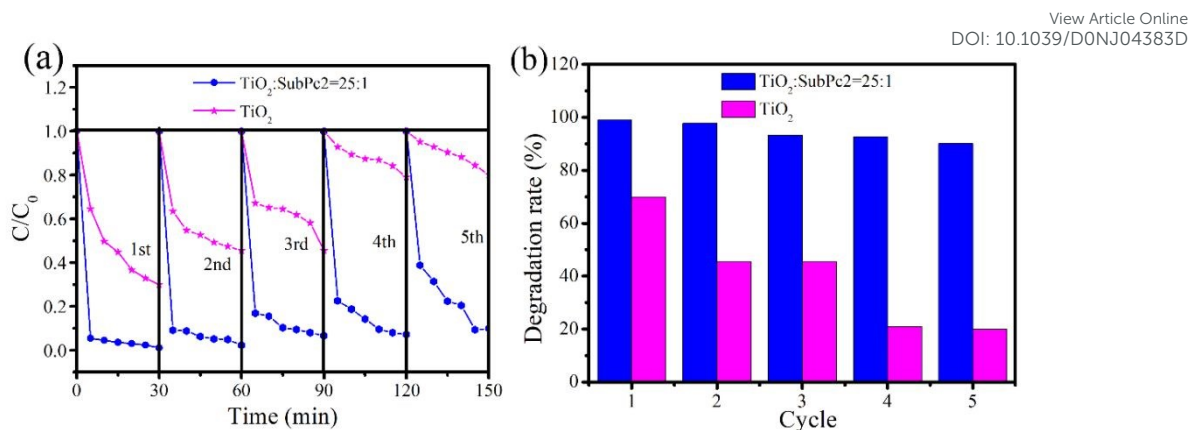


Fig. 8. Cyclic stability of the TiO_2 /SubPc2 (25:1) for the degradation of BB under visible light irradiation.

The reusability and stability of catalysts are important advantages of all photocatalysts. To evaluate the catalyst stability, the TiO_2 /SubPc2 (25:1) was employed to degrade BB for 5 cycles under visible light irradiation. After every cycle, catalysts were rinsed with distilled water and ethanol, and then dried in an oven at 60 °C for 3 h to ensure it can be used for the next degradation experiments. From Fig. 8 (b), we can find that the degradation rate is still very high (90.11%) during the five cycles, which is 4.5 times compared with pure TiO_2 . We assume that the reduction of catalytic activity attribute to the cover of these photocatalysts surface with the byproducts or adsorbed dyes after degradation experiments. The results illustrate that the prepared TiO_2 /SubPc exhibits excellent recyclability and photostability.

4. Conclusion

In this paper, we had successfully synthesized TiO_2 /SubPc2 photocatalysts with different concentrations and evaluated the degradation potential of MO, BB, MB, and AM under visible light irradiation. The axial substituted subphthalocyanine with p-hydroxybenzaldehyde oxy was obtained using a simple solvothermal approach in the toluene solution.

The results showed that the TiO₂/SubPc2 composite photocatalysts with different concentrations exhibited excellent photocatalytic performance than the pure TiO₂. For all organic dyes, the optimal photodegradation ratio is TiO₂:SubPc2 = 25:1. Meantime, the values of the calculated release rate constants increased with the addition of SubPc2. The cyclic stability experiments indicated that the photodegradation rate of BB by TiO₂/SubPc2 (25:1) after five cycles can still very high reached (90.11%) that it had good cycle stability. Our present work shows that TiO₂/SubPc could be widely developed in the degradation of pollutants in water, which lay down the foundations for the high-performance photocatalysts in future research.

Conflicts of interest

There are no conflicts of interest to declare.

Acknowledgments

This work was supported by the National Natural Science Foundation of China (21606180), the Natural Science Foundation of Shaanxi Provincial Education Department (16JK1786 and 16JF027), and the Foundation of China Scholarship Council (201906970011).

References

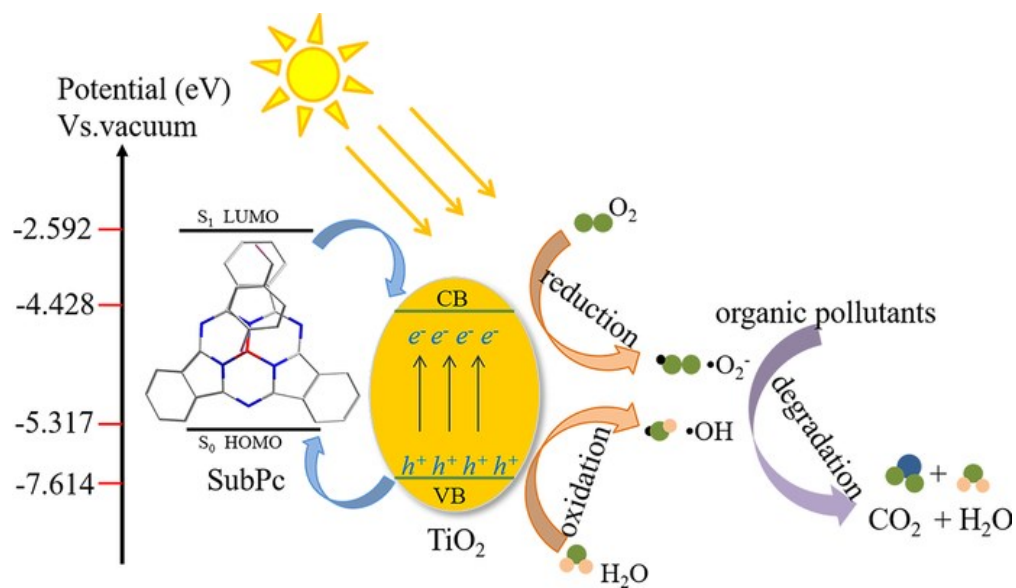
- 1 J. Singha, S. Kumara and R Ashis, *Opt. Mater.*, 2020, **17**, 110138.
- 2 M. Bacanli and N, Başaran, *Food Chem. Toxicol*, 2019, 125.
- 3 W. L. Kebede, D. H. Kuo and F. T. Beken, *Chemosphere*, 2020, **254**, 126823.
- 4 S. Gorduk, O. Avciata and U Avciata, *Inorg. Chim. Acta, Rev.*, 2018, **471**, 137-147.
- 5 T. Cai, Y. T. Li, L. L. Wang, S. Q. Zhan, W. Y. Donga, H. Chen, J. H. Ma, C. B. Liu and S. L. Luo, *J. Colloid Interface Sci.*, 2018, **533**, 95-105.

- 1
2
3
4
5
6
7
8
9
10
11
12
13
14
15
16
17
18
19
20
21
22
23
24
25
26
27
28
29
30
31
32
33
34
35
36
37
38
39
40
41
42
43
44
45
46
47
48
49
50
51
52
53
54
55
56
57
58
59
60
- 6 R. Piotr, S. Bartosz and G Jace, *Biochem, Eng. J.*, 2019, **141**, 146-162.
- 7 S. Gunti, A. Kumar and M. K. Ram, *Int. Mater. Rev.*, 2018, **63**, 257-282.
- 8 Y. Y. Yue, X. H. Wang, Q. L. Wu, J. Q. Han and J. C. Jiang, *J. Colloid Interface Sci.*,
2019, 564.
- 9 R. Ivan, A. P. Pino, I. Yousef, C. Logofatu and E. György, *J. Photochem. Photobiol., A*,
2020, **399**, 112616.
- 10 B. G. Alhogbi, M. Aslam, A. Hameed and M. T. Qama, *J. Hazard. Mater.*, 2020, 397.
- 11 A. R. Arul, T. E. Manjulavalli and R. Venckatesh, *Mater. Today: Proc.*, 2019, **18**,
1760-1769.
- 12 A. Najafidoust, S. Allahyari, N. Rahemi and M. Tasbihi, *Ceram. Int.*, 2020, **46**,
4707-4719.
- 13 Z. Li, B. Wang, G.Y. Cui, B.B. Zhang, Y.F. Wang, L. Yang, H.X. Ma, L.Y. Jiao, L.Y.
Pang and X.X. Ma, *J. Alloys Compd.*, 2021, **855**, 157458.
- 14 D. Boczara, T. Łęckia and M Skompska, *J. Electroanal. Chem.*, 2020, **859**, 113829.
- 15 F. C. Lopes, M Rocha, P. Bargiela and H. S. Ferreir, *Chemical Engineering ence*, 2020.
- 16 Y. J. Yan, M. Yang, H. Shi, C. J. Wang, J. Fan, E. Z. Liu and X. Y. Hu, *Ceram. Int.*,
2018.
- 17 M. C. Wu, W. K. Huang, T. H. Lin and Y. J. Lu, *Appl. Surf. Sci.*, 2018, 469.
- 18 A. Truppi, F. Petronella, T. Placido, V. Margiotta, G. Lasorella, L. Giotta, C. Giannini,
T. Sibillano, S. Murgolo, G. Mascolo, A. Agostiano, M. L. Curri and R. Comparelli,
Appl. Catal., B, 2019, **243**, 604-613.
- 19 S. T. Kochuveedu, Y. H. Jang and D. H. Kim, *Chem, Soc. Rev*, 2013, **42**, 8467-8493.

- 1
2
3
4
5
6
7
8
9
10
11
12
13
14
15
16
17
18
19
20
21
22
23
24
25
26
27
28
29
30
31
32
33
34
35
36
37
38
39
40
41
42
43
44
45
46
47
48
49
50
51
52
53
54
55
56
57
58
59
60
- 20 T. Alessandra, P. Francesca and P. Tizian, *Catal.*, 2017, **7**(12), 100.
- 21 G. B. Dinda, Z. Ahin, H. C. Yatma and U. Isci, *J. Porphyrins Phthalocyanines*, 2019,
23(4n05), 1-8.
- 22 N. Li, Z. X. Sun, R. Liu, L. Xu, K. Xu and X. M. Song, *Sol. Energy Mater. Sol. Cells*,
2016, **157**, 853-860.
- 23 Z. Z. Fan, L. F. Fan, S. M Shuang and C. Dong, *Talanta*, 2018, **189**, 16-23.
- 24 X. B. Li, T. Zhang, Y. B. Chen, Y. M. Fu, J. Z. Sun and L. J. Guo, *Chem. Eng. J.*, 2020,
382, 122783.
- 25 B. Wang, G. Y Cui, Z. Li, H. X. Ma and B. B. Zhang, *Mater. Today Commun.*, 2020,
25, 101264.
- 26 B. Wang, G. Y Cui, B. B. Zhang, Z. Li, H. X. Ma, W. Wang, F. Y. Zhang and X. X. Ma.
Opt. Mater., 2020, **109**, 110202.
- 27 B.B. Zhang, H. Hao, F.Y. Zhang, B. Wang, J. Xue, L.Y. Jiao and Z. Li, *J. Appl.*
Electrochem., 2020.
- 28 Q. Xu, Y. Gao, X. F. Wu, H. Hang, H. Li, Y. H. Chen, W. J. Wang and H. Tong, *New J.*
Chem., 2019, **43**, 16385-16390.
- 29 Z. Li, B. Wang, B.B. Zhang, G.Y. Cui, F.Y. Zhang, L. Xu, L.Y. Jiao, L.Y. Pang and
X.X. Ma, *ChemistryOpen*, 2020, **9**, 1001-1007.
- 30 E. M. Graham and P. B. Timothy. *ACS Appl Mater Interfaces.*, 2012, **4**(10), 5055-68.
- 31 A. Şenocak, T. Basova, E. Demirbas and M. Durmuş, *Electroanalysis*, 2019, **31**, 1-12.
- 32 Z. Li, B. Wang, B.B. Zhang, H.X. Ma, J. Xue, L. Xu, L.Y. Jiao, X.X. Ma, *J. Photochem.*
Photobiol., A, 2021, **405**,112929.

- 1
2
3
4
5
6
7
8
9
10
11
12
13
14
15
16
17
18
19
20
21
22
23
24
25
26
27
28
29
30
31
32
33
34
35
36
37
38
39
40
41
42
43
44
45
46
47
48
49
50
51
52
53
54
55
56
57
58
59
60
- 33 M. J. Frisch, G. W. Trucks, H. B. Schlegel, G. E. Scuseria, M. A. Robb, J. R. Cheeseman, G. Scalmani, V. Barone, G. A. Petersson, H. Nakatsuji, X. Li, M. Caricato, A. V. Marenich, J. Bloino, B. G. Janesko, R. Gomperts, B. Mennucci, H. P. Hratchian, I. V. Ortiz, A. F. Izmaylov, J. L. Sonnenberg, Williams, F. Ding, F. Lipparini, F. Egidi, J. Goings, B. Peng, A. Petrone, T. Henderson, D. Ranasinghe, V. G. Zakrzewski, J. Gao, N. Rega, G. Zheng, W. Liang, M. Hada, M. Ehara, K. Toyota, R. Fukuda, J. Hasegawa, M. Ishida, T. Nakajima, Y. Honda, O. Kitao, H. Nakai, T. Vreven, K. Throssell, J. Montgomery, J. E. Peralta, F. Ogliaro, M. I. Bearpark, J. Heyd, E. N. Brothers, K. N. Kudin, V. N. Staroverov, T. A. Keith, R. Kobayashi, J. Normand, K. Raghavachari, A. P. Rendell, J. O Burant, S. S. Iyengar, J. Tomasi, M. Cossi, J. M. Millam, M. Klene, C. Adamo, R. Cammi, J. W. Ochterski, R. L. Martin, K. Morokuma, O. Farkas, J. B. Foresman and D. J. Fox, Gaussian, Inc., Wallingford, CT, 2009.
- 34 W. Humphrey, A. Dalke and K. J. Schulten, *J. Mol. Graph. Model*, 1996, **14**, 33-38.
- 35 T. Lu and F. W. Chen, *J. Comput. Chem*, 2012, **33**, 580-592.
- 36 X. S. Huang, M. Hu and X. H. Zhao, *Org. Lett.* 2019, **21**, 3382-3386.
- 37 J. B. Arockiam and S. Jong, *Spectrochim. Acta, Part A*, 2018.
- 38 M. Shaban, A. M. Ahmed, N. Shehata, M. A. Betiha and A. M. Rabie, *J. Colloid Interface Sci.*, 2019, **555**, 31-41,
- 39 S. Ding, D. Mao, S. Yang, F. Wang, L. Meng, M. Han, H. He, C. Sun, B. Xu, *Appl Catal.B: Environ.*, 2017, **210**, 386-399.
- 40 A. A. Abdel-Khalek, S. A. Mahmoud, A. H. Zak. *Environmental Nanotechnology, Monitoring & Management*, 2018, **9**, 164-173.

- 1
2
3
4 41 M. Goswami, D. Baruah and A. M. Das, *New J. Chem.*, 2018, **42**, 10868-10878
5
6
7 42 I. Fatimah, E. Z. Pratiwi and W. P. Wicaksono, *Egypt. J. Aquat. Res.*, 2020, **46**, 35-40.
8
9
10 43 H. Noreen, J. Iqbal, A. Arshad, R. Faryal, A. Rahman and R. Khattak, *J. Solid State*
11
12 *Chem.*, 2019, **275**, 141-148.
13
14
15 44 G. P. Costa, R. A. Rafaela, J. C. Serpa Soares and A. B. Gaspar, *Catal. Today*, 2020,
16
17 **344**, 240-246.
18
19
20 45 V. N. Sonkusare, R. G. Chaudhary, G. S. Bhusari, A. Mondal, A. K. Potbhare, R. K.
21
22 *Mishra, H. D. Juneja, A. A. Abdala. ACS Omega*, 2020, **5**, 7823-7835.
23
24
25
26
27
28
29
30
31
32
33
34
35
36
37
38
39
40
41
42
43
44
45
46
47
48
49
50
51
52
53
54
55
56
57
58
59
60



58x33mm (300 x 300 DPI)